Earth and Environmental Science Transactions of the Royal Society of Edinburgh, **111**, 235–245, 2021 (for 2020)

Article

The influence of climatic conditions on the permeability and hydraulic properties of the L_5–S_5 layers in the Loess Plateau, North Qinling Mountains

Yao CHEN[1,2]*, Hui QIAN[2] and Kai HOU[2]

[1] Electric Power Research Institute, State Grid Fujian Electric Power Company Limited
[2] School of Environmental Science and Engineering, Chang'an University, Xi'an, China
*Corresponding author. Email: chenyao3715@chd.edu.cn

ABSTRACT: A better understanding of the role of Quaternary-era climate change in the development of regional hydrology in the Loess Plateau and the impact on regional ecosystems is needed. In particular, a thorough examination of the permeability and recharge under different conditions in the fifth loess–palaeosol layer is required. The fifth loess–palaeosol layer is located at the southern edge of the Jinghe River in the Guanzhong Basin, and was examined to better understand these conditions. A constant head permeability test was conducted at 11 points that covered different stratum of loess–palaeosol, and 55 corresponding undisturbed soil samples were analysed for porosity, magnetic susceptibility, and grain size. Results showed that: (1) with an increase in hydraulic gradient, the permeability coefficient of the upper part of the loess and the lower part of the palaeosol showed contrasting characteristics – this phenomenon was closely related to climatic conditions during the sedimentary period, post-sedimentary microbial activity, and to certain properties relating to permeability in the strata under similar monsoon effects; (2) the Loess Plateau, alternately dominated by the East Asian summer and winter monsoons, exhibited different grain-size compositions in the sedimentary layer, which, in turn, made the permeability in the loess noticeably more stable than that in the palaeosol; and (3) different aquifer characteristics and recharge conditions between the loess–palaeosol layers can be primarily explained by the intensity of the pedogenesis, which depended on extreme dry-old glacial climates and relatively humid-warm interglacial climates. These findings show that climate change played an important role in influencing hydrological systems in the loess–palaeosol sequence.

KEY WORDS: climate change, loess–palaeosol, permeation law, regional hydrology.

For over half a century, scholars have been studying Quaternary sediments and associated environmental information, making significant achievements (Allen *et al*. 1999; Lu *et al*. 2004; Gorbarenko *et al*. 2007; Rao *et al*. 2013; Chen *et al*. 2020a, b). In particular, the loess–palaeosol sequence on the Loess Plateau in China is considered one of the three major global cornerstones for research on Quaternary climate change because of its sensitivity to paleoclimatic environment changes and the detailed records available about the strata (Chen *et al*. 2008; Peng *et al*. 2014; An *et al*. 2015; Liu *et al*. 2015; Wang *et al*. 2019a, b). Over time, research on the Loess Plateau has made significant contributions to revealing the climatic evolution of East Asia and the world (Kukla & An 1989; Liu & Ding 1998; Balsam *et al*. 2004; Torrent *et al*. 2007). However, only a few studies have observed changes in the hydraulic properties of the sedimentary sequence in the Loess Plateau that resulted from Quaternary climate change (Chen *et al*. 2016, 2017; Chen & Qian 2017). Many scholars have focused only on the source, migration, water-chemical properties, and occurrence of groundwater in the loess. Previous studies have found that atmospheric precipitation is the only source of supply; groundwater in the loess occurs in various forms, including capillary, pore, and fracture water, and the chemical properties of groundwater have considerable influence on the regional environment (Qian & Li 2011; Huang *et al*. 2013; Li *et al*. 2013a, b; Liu *et al*. 2015; Wang *et al*. 2019a, b). However, differences in percolation between the loess–palaeosol sequences have rarely been examined with high accuracy. Consequently, it is necessary to accurately measure the relationships among levels of aquifer development in the Loess Plateau, the causes of such differences, and the effects of Quaternary climate change.

The Shaanxi Guanzhong Basin is a major granary in the north-western part of China; it has a well-deposited loess–palaeosol sedimentary sequence and rich groundwater resources (Wang *et al*. 2007; Pan *et al*. 2015; Zhao *et al*. 2017; Wu *et al*. 2019). Identifying the relationships between the differences in the hydraulic properties of the loess–palaeosol sequences and the environment is significant in order to conserve and restore the ecosystem in the Loess Plateau while sustainably building its industrial and agricultural development more effectively.

The S_5 formation on the Loess Plateau is the most obvious stratum in the Quaternary loess strata in China because of its extremely thick deposition, characteristic colour, and strong soil microstructure. The fifth palaeosol, S_5, was formed under subtropical humid-warm conditions and is the most noticeable regional marker bed for the Loess Plateau and is equivalent to the 13th–15th marine isotope stages, as shown in the deep-sea-deposited oxygen isotope curve (Ruddiman *et al*.

 doi:10.1017/S1755691020000110
https://doi.org/10.1017/S1755691020000110 Published online by Cambridge University Press

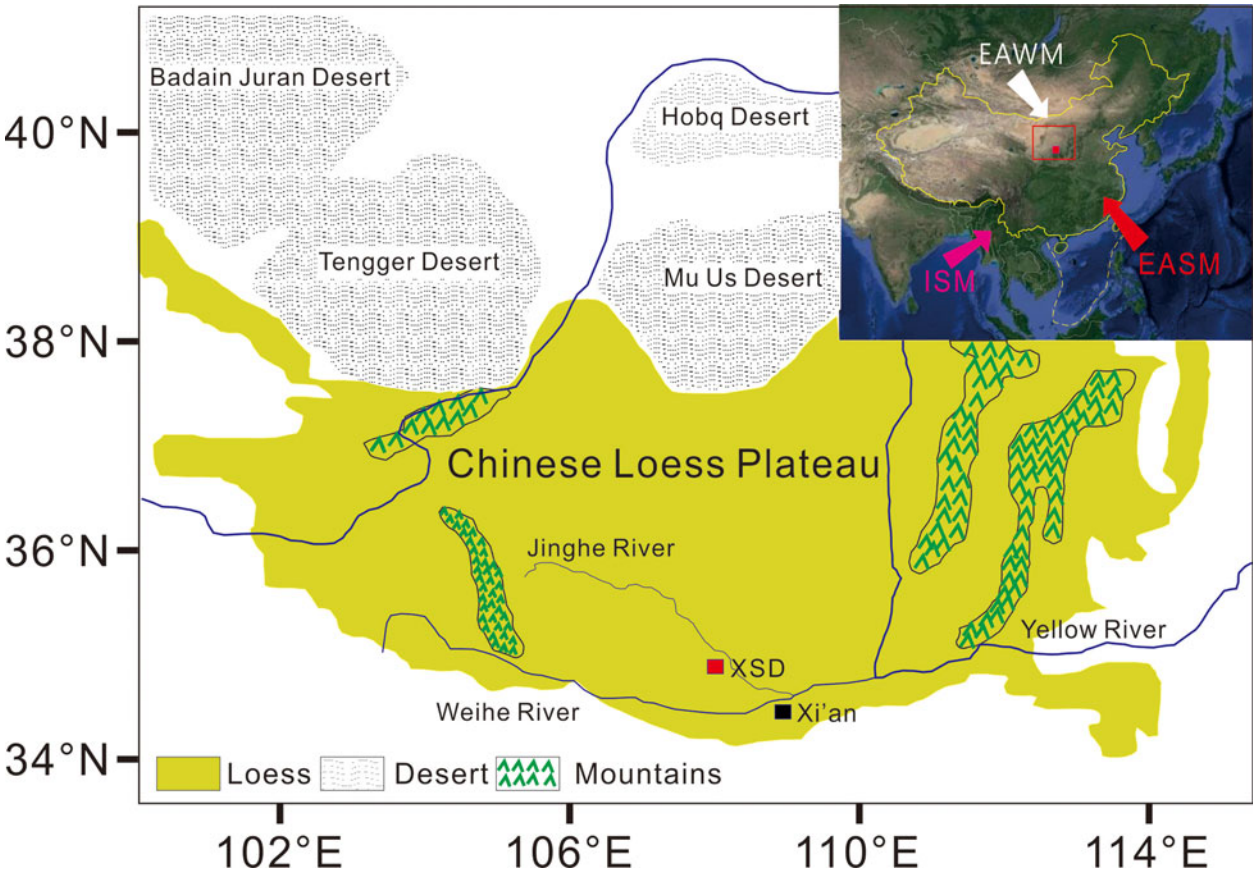

Figure 1 The location of the Loess Plateau and studied sections. Abbreviations: EAWM = East Asian winter monsoon; EASM = East Asian summer monsoon; ISM = Indian Ocean summer monsoon.

1989; Thomas *et al*. 2007; Wu & Qian 2016). Compared with the average temperature since 1950, temperatures in the Quarternary were 4–6°C higher, with 200–300 mm more annual precipitation (Kukla *et al*. 1998). The overlying fifth Malan loess, L_5, is believed to have been deposited under an extremely dry-cold climate (Liu & Ding 1998; Song *et al*. 2014; Wu *et al*. 2018). The differences between the two sedimentary environments lead to variations in physical properties, which may, in turn, cause similarities and variations in the chemical-physical properties of the strata.

On the basis of these observations, the relationships between the magnetic susceptibility and grain-size composition (indices that reflect climate change) of the fifth layer of the loess–palaeosol sequences and the differences in the water-chemical properties in the strata of the Xiushidu (XSD) Quaternary profile at the southern edge of Jinghe River in Guanzhong Basin, China, were examined through field survey, sampling, and laboratory experimentation. The purpose of these experiments in loess–palaeosol was to: (1) compare the permeability characteristics and the related causes under different hydraulic gradients; (2) determine differences in permeability under different paleoclimatic environments and reveal their causes; and (3) define recharge conditions and identify factors in different aquifers that impact those conditions.

1. Geographical and geochronological background

The XSD loess–palaeosol at the southern edge of the Jinghe River is located in Guanzhong Basin [108°29′40″E, 34°26′37″N] (Fig. 1), 26.2 km N from Xi'an. The study area features a warm temperate continental monsoon climate and four distinct seasons with both rain and high temperatures during the same period. The annual average temperature since 1950 is 13 °C, the lowest temperature in winter was −20.8 °C, and the highest temperature in summer reached 41.4 °C. The annual average rainfall since 1950 is approximately 548 mm, the mean annual sunshine duration is 2195.2 h, with the longest duration in August of 241.6 h. Field sampling for this study was conducted from late August to early October in 2017.

The XSD Quaternary loess–palaeosol sequences are well-deposited, with a sedimentary thickness of approximately 57 m. According to field observations, the fifth Malan loess (L_5) and the palaeosol (S_5) are well-preserved, with a depositary depth of about 11 m and no observed remarkable sedimentary discontinuities (Fig. 2). From top to bottom, the colour in L_5 changed as follows: dark yellowish brown (YR-20-10YR4/4), yellowish brown (YR-20-10YR5/4), light yellowish brown (YR-20-10YR6/4), yellowish brown (YR-20-10YR5/4), and dark yellowish brown (YR-20-10YR4/4). L_5 has loose soil, with a dry density of 1.72–1.77 g m^{-3} and a moisture content of 4–16 %. It also has a baum pot and snail shells with a few grey-brown spots and a small number of calcareous nodules at the top. The physical and chemical properties of the underlying palaeosol (S_5) formed in the same climate cycle are different in all aspects from those of L_5, with a dry density and moisture content that are slightly higher than those of L_5. The thickness of S_5, as the most noticeable marker bed in the loess, reaches 4 m, and its colour changed as follows (from top to bottom): yellowish brown (YR-20-10YR5/4), brown (YR-17-7.5YR4/4), yellowish brown (YR-20-10YR5/4), and brown (YR-17-7.5YR4/4). This colour change shows the strength of the pedogenesis. As seen in Figure 3, S_5 can be divided into three layers. The figure also shows the typical yellow-brown soil found in northern subtropical forests. From top to bottom, the first layer is the clarification layer (Bts), which has many baum pots and a grain size of 5–13 mm, is densely distributed, and contains many iron–manganese

https://doi.org/10.1017/S1755691020000110 Published online by Cambridge University Press

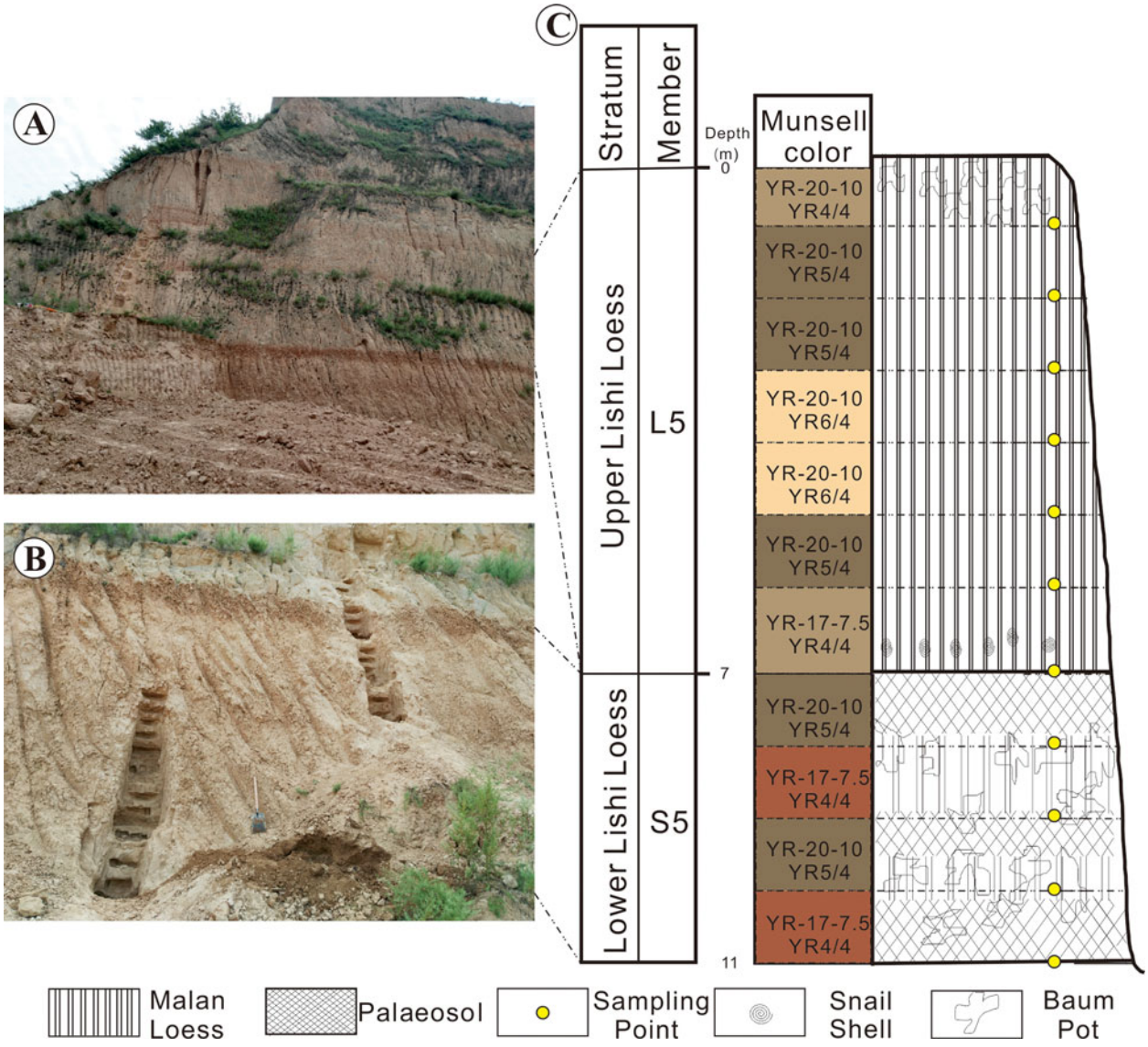

Figure 2 Field photos of the XSD profile: (A) L_5, and (B) S_5. (C) Framework of the XSD section.

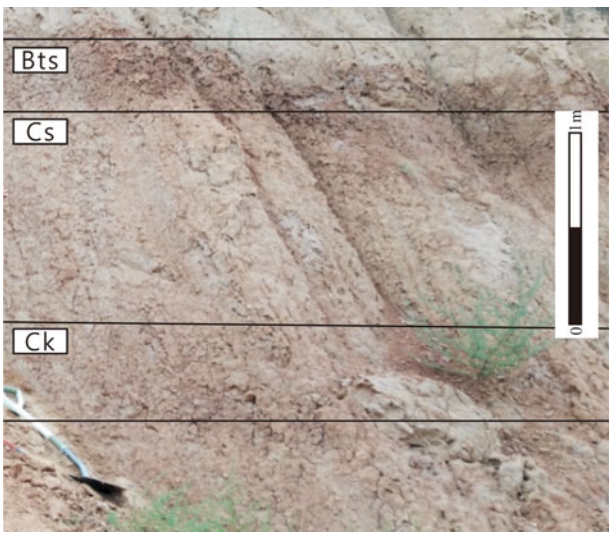

Figure 3 Subdivision of a section of the S_5 palaeosol at the XSD. Abbreviations: Bts = argillic horizon; Cs = leached loess with thin red argillans; Ck = illuvial layer of $CaCO_3$.

cutans, indicating that this layer was formed under high temperatures and precipitation, and was subjected to strong clarification. The second layer is the weathering-leaching layer (Cs), which has a denser distribution of baum pot. Because this distribution is star-like, it is often referred to as 'reticular baum pot,' and has a grain size of 1–2 cm. Compared to L_5, its soil is harder (given its dense structure) and deposited like a prism block. The third layer is the calcium carbonate ($CaCO_3$) nodule sedimentary layer (Ck). Compared to Cs, the content of baum pot significantly increases, which further indicates that Bts was deposited under a humid climate and was subject to a strong leaching effect.

2. Sampling and analytical methods

2.1. Sampling

Three trench sampling areas were provided in different layers of the XSD profile through the field survey located in the Loess Plateau slope: L_5 (7 m), S_{5-1} (1 m), and $S_{5-2,3}$ (3 m). To ensure that the samples taken from the field were closer to their state during the sedimentary period to the extent possible, the weathered topsoil from 1–2 m inside the slope was removed before the

https://doi.org/10.1017/S1755691020000110 Published online by Cambridge University Press

trenches were dug downward from the top of the respective layers. Loose soil samples weighing 1.5 kg each were acquired from each trench at 10 cm intervals and analysed for magnetic susceptibility, grain size, moisture content, and specific gravity. At each sampling point, three vertical and three horizontal samples were collected by cutting rings with heights and diameters of 40 and 61.8 mm, respectively, for a total of 66 samples. The dry density of each sample was recorded on site and numbered according to the strata sequence.

2.2. Dry density determination

Prior to sampling, each cutting ring was weighed as m_0, accurate to 0.01 g. After the preparation of the field permeation sample, the soil-loaded cutting ring was reweighed as m_1, accurate to 0.01 g. The dimensions of the cutting ring were 61.8 mm (inner diameter) and 40 mm (height), resulting in an inside volume, V, of 120 cm^3 and a dry density soil sample of:

$$\rho_d = \frac{m_1 - m_0}{V} \tag{1}$$

2.3. Indoor penetration test

The permeation samples were brought to the laboratory where their saturated soil hydraulic conductivity coefficients were measured. A water supply tank, piezometric tube, and permeameter related to rubber hoses. The tank was filled with water after all connections were found to have no water or gas leakages. Then, Vaseline was applied on the inner walls of the TST-55 Permeameter, and field samples were placed into the designated permeameter in numbered order. The permeameter was tightened according to specifications to ensure they did not overflow. A stepwise lifting method was employed to ensure that the samples were fully saturated. A constant head permeability test was carried out until the samples were fully saturated. The hydraulic gradient (I) for the constant head permeability test was: 0.1, 0.2, 0.3, 0.4, 0.5, 0.6, 0.7, 0.8, 0.9, 1, 1.5, 2, 2.5, 3, 3.5, 4, 4.5, 5, 6, 7, 8, 9, and 10, for a total of 23 hydraulic gradients. After the head reached the corresponding water level, the piezometric tube head was observed for stability, which should be no less than 30 min from the starting time. The water was held with a graduated cylinder, and when the amount of water seeping out was 2/3 greater than the graduated cylinder level, the graduated cylinder was removed, the corresponding time was recorded, the mass of water was weighed with an electronic scale, and the water temperature of the tank was measured. Afterward, five groups of constant head permeability tests were performed, and the corresponding height needed to reach the required hydraulic gradient was raised until either 23 hydraulic gradients were recorded or the soil samples were damaged. The amount of water that seeped out during each hydraulic gradient was read only after the piezometer tube was stabilised to ensure that the test was conducted under constant head.

$$k_{20} = k_T \frac{\eta_T}{\eta_{20}} \tag{2}$$

Permeability, k_{20} (cm s^{-1}), was calculated for samples at a standard temperature, where: η_T is the coefficient of water dynamic viscosity (kPa·s) at T °C; and η_{20} is the coefficient of water dynamic viscosity (kPa·s) at 20 °C.

2.4. Determining the specific gravity of the soil sample

The specific gravity of the soil samples was determined using the pycnometer test method with reference to the Standard for Soil Test Method (GB/T50123-1999). Loose soil was obtained from field permeation sampling points, brought back to the laboratory, placed in an oven, and dried to a constant weight at a constant temperature of 105–110 °C. Given that a 50 ml pycnometer was used, approximately 10 g of the dried samples were weighed and transferred into the pycnometer. The total mass of the samples and the pycnometer were accurately weighed to 0.001 g, then approximately half of the pycnometer was filled with kerosene. The pycnometer was then shaken and evacuated using the vacuum extraction method for no less than one hour. After the vacuum extraction was completed, the pycnometer was filled with the suspension. Given that the pycnometer had a narrow neck, it was filled with kerosene and corked. The excess kerosene overflowed from the capillary. The pycnometer was kept still until the supernatant became clear; then, kerosene was removed from the outer walls and the total mass of the pycnometer, water, and samples were weighed, accurate to 0.001 g. The specific weight of the soil grains (G_s) can be calculated as:

$$G_s = \frac{m_d}{m_{bw} + m_d - m_{bws}} \cdot G_{\text{kerosene}} \tag{3}$$

where m_{bw} is the total mass of the pycnometer and kerosene (g) and m_{bws} is the total mass of the pycnometer, kerosene, and samples (g).

2.5. Porosity calculation

The porosity of permeation samples (F) was calculated according to the measured specific weight and dry weight of soil samples:

$$F = 1 - \frac{\rho_d}{G_s} \tag{4}$$

2.6. Magnetic susceptibility measurement

As opposed to the two previous samples, the loose soil samples tested for magnetisability and particle size were dense. A total of 55 samples were taken at an average interval of 20 cm from top to bottom. The collected loose soil samples were dried under natural indoor conditions. After air drying at a constant temperature for 48 h, approximately 10 g of the samples were ground into powder and placed into plastic bags. The samples were preheated at low frequency for 30 min (χ_{lf}) (0.47 kHz). Then, the exact quantity was weighed, and a Magnetic Susceptibility Model-942 magnetic susceptibility meter (made in China) was used to take measurements. Before measurement, the instrument was placed away from the magnetic field.

2.7. Grain-size analysis

For the particle size analysis test, a Mastersizer 2000 laser particle size analyser (Malvern, UK) was used, which has a range of 0.02–2000 μm and a repeat test error of less than 1 %. Samples were treated with hydrochloric acid and hydrogen peroxide before testing to remove carbonate, organic matter, and iron oxide. Dispersant was added to the treated samples, which were then subjected to ultrasonic shaking for five minutes.

3. Results

3.1. Basic physical properties of loess

The measurement results for the basic physical properties of the XSD profile are shown in Figure 4. During the evolution from L_5 to S_5, the dry density gradually increased with stratum depth. Similar to variations in dry density, the specific weight of grains tended to increase but had greater variability. By contrast, the porosity values of the permeation samples gradually decreased with stratum depth. Porosity was calculated with the results of dry density and specific weight of the soil grains. For L_5, the mean porosity value was 31.58 %, with a range of 28.56–35.01 %. In general, the porosity of L_5 was approximately 5 % higher than that of S_5, indicating that the L_5 aquifer should, theoretically, be more well-deposited than that of S_5.

https://doi.org/10.1017/S1755691020000110 Published online by Cambridge University Press

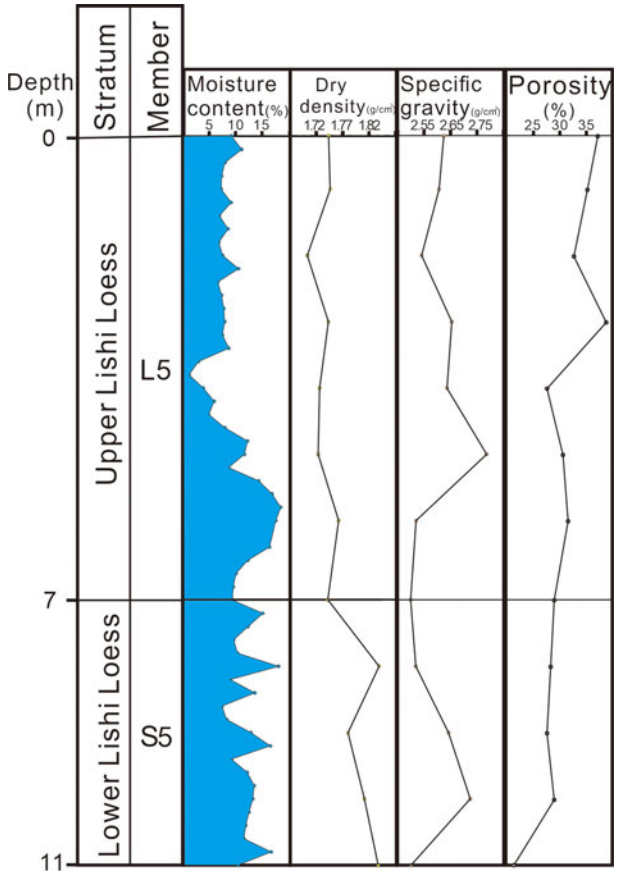

Figure 4 The moisture content, dry density, specific gravity, and porosity from L_5–S_5 of a loess section in the XSD.

3.2. Penetration test results

According to the results of the indoor constant head permeation test, the permeability for L_{5-1}, L_{5-2}, and L_{5-3} (depths of 1, 2, and 3 m from the original surface of the fifth Malan loess) decreased horizontally and vertically as I increased. When $I < 4$, the permeability was greater. After $I > 4$, the permeability stabilised.

In contrast to the above, when $I \leq 2$, the permeability for L_{5-4} (depth of 4 m from the original surface of the fifth Malan loess) gradually decreased as I increased. When I ranged from 2–4, permeability stabilised, but after 4, it increased (Fig. 5; L_{5-4}).

The permeability for L_{5-5} (depth of 5 m from the original surface of the fifth Malan loess) was different from all the above points. Both horizontal and vertical permeability were stable as I varied, although it generally increased (Fig. 5; L_{5-5}).

The horizonal and vertical permeability for L_{5-6} and L_{5-7} (depths of 6 and 7 m from the original surface of the fifth Malan loess) had high variability and followed no noticeable trend as I increased (Fig. 5; L_{5-6}, L_{5-7}).

The horizonal and vertical permeability of S_{5-1} and S_{5-2} (depths of 8 and 9 m from the original surface of the fifth Malan loess) were like that of the overlying loess, and were highly volatile as I increased. However, in general, they were significantly smaller than that of the overlying loess (Fig. 6; S_{5-1}, S_{5-2}).

The vertical and horizontal permeability for S_{5-3} in the middle of the fifth palaeosol (depth of 1 m from the original surface of the fifth Malan loess) and S_{5-4} in the lower part of the fifth palaeosol (depth of 11 m from the original surface of the fifth Malan loess) had the same relationship with I as the upper part of L_5.The permeability gradually decreased as I increased. The difference was that the permeability at the test points in the lower middle part of S_5 was significantly less than that in the Malan loess. When $I = 4$, S_{5-3} was readily stable, but it was not until $I = 6$ that S_{5-4} became stable (Fig. 6; S_{5-3}, S_{5-4}).

These results were analysed statistically to examine the stability of the permeability across the loess–palaeosol sequence, which changed with the hydraulic gradient during the permeability test and the average permeability (Fig. 7). This finding suggested that the vertical and horizontal equivalent permeability for the entire fifth loess–palaeosol sequence were 0.0067 and 0.075 m d^{-1}, respectively. Nearly all layers with permeability less than this average value were in S_5. Only the average vertical permeability in L_{5-7} was abnormal according to the analysis of the coefficient values of permeability, which changed as the hydraulic gradient increased. In this analysis, when the coefficient of variation was less than 17, this relationship was relatively stable (Wang *et al.* 2018). Over 70 % of the test points in L_5 had large variability coefficients of permeability, and maximum values appeared in the transition zone between L_5 and S_5, while only part of the middle of L_5 (vertical direction) and S_5 (horizonal direction) had smaller variability.

In summary, the permeability under the initial hydraulic gradient was regarded as the initial permeability. The representative data for the initial permeability (A), the pre-stabilising permeability (B), and the post-stabilising permeability (C) are listed in Table 1.

Table 1 illustrates that A, B, and C first increased then decreased as the profile depth increased in both the vertical and horizontal directions of the fifth loess–palaeosol sequence. Maximum values appeared in L_{5-4} at three points. Below L_{5-6}, the stratum permeability plummeted. A responded to the depth of stratum, and decreased from 0.33 to 0.001 m d^{-1} in the vertical direction, while in the horizontal direction, A decreased from 0.19033 to 0.0010.33 m d^{-1}.

3.3. Measurement of susceptibility and particle size results

As seen in Figure 8, L_5 and S_5 were significantly different in magnetic susceptibility. The magnetic susceptibility of L_5 changed more moderately than that of S_5. An abrupt change point appeared at the bottom of L_5 and went deep into S_5 along the stratum. The magnetic susceptibility gradually increased, and periodic minimum values appeared at S_{5-2}. The mass susceptibility of L_5 ranged from 4.55 to 11.23 SI, whereas that of S_5 ranged from 8.35 to 21.76 SI. The magnetic susceptibility measurements showed that the effect of weathering and soiling on L_5 was weaker than that on S_5, which provides a basis for identifying the relationships between the water-chemical properties of L_5 and S_5, differences in physical properties, and climate change.

For grain size, as shown in Figure 9, as the stratum went deeper, the grain-size distribution of L_5 and S_5 showed significance differences. In L_5, the average content of clay, fine-silty sand, coarse silt, and microsand were 23.87 %, 19.08 %, 55.46 %, and 1.58 %, respectively, while their ranges were 14.91–35.31 %, 15.19–24.49 %, 40.05–65.96 %, and 0.18–3.93 %, respectively. In S_5, the average contents of clay, fine-silty sand, coarse silt, and microsand were 31.97 %, 22.50 %, 44.99 %, and 0.52 %, respectively, while their ranges were 21.80–40.43 %, 18.57–28.17 %, 35.36–57.32 %, and 0.19–1.71 %, respectively.

When L_5 and S_5 were compared, the content of clay and fine-silty sand in L_5 was 12 % lower than that in S_5, whereas the content of coarse silt and microsand in L_5 was 12 % higher than that in S_5. Some research used the ratio of percentage content of grains that are smaller than 2 μm and greater than 10 μm as an alternative index for measuring changes in climate (Lu *et al.* 2004; Fu *et al.* 2018). The magnetic susceptibility curves were compared to identify their correlation, which, in turn, further demonstrated the influence of climate change on grain-size composition. While not the only factor, climate may have caused different physical and hydraulic properties in L_5 and S_5.

https://doi.org/10.1017/S1755691020000110 Published online by Cambridge University Press

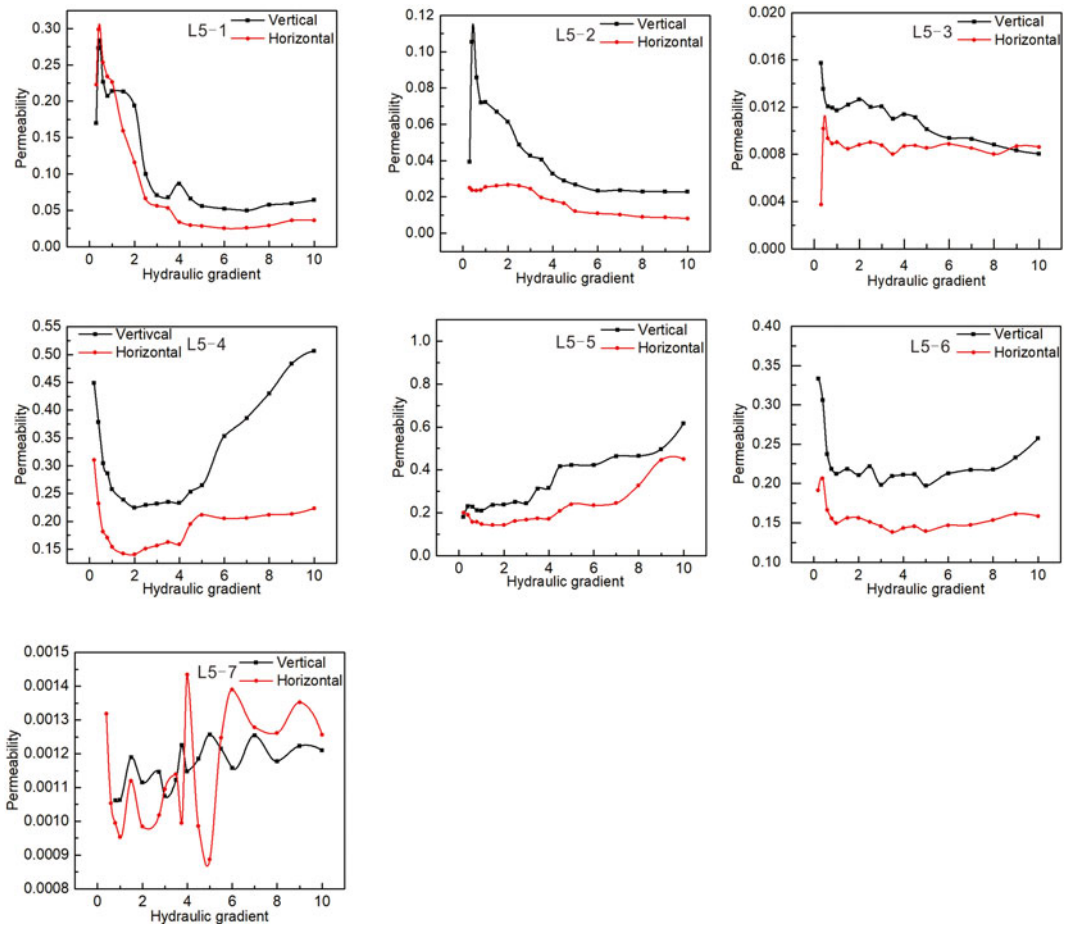

Figure 5 The permeability coefficient varied with the hydraulic gradient from L_{5-1} to L_{5-7} in the XSD.

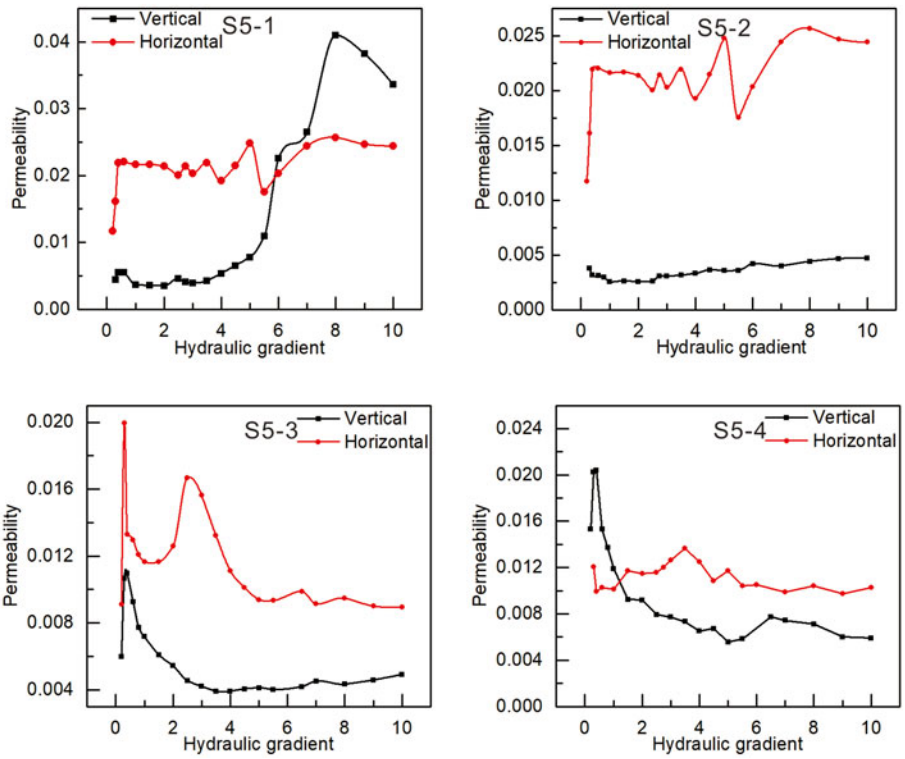

Figure 6 The permeability coefficient varied with the hydraulic gradient from S_{5-1} to S_{5-4} in the XSD.

https://doi.org/10.1017/S1755691020000110 Published online by Cambridge University Press

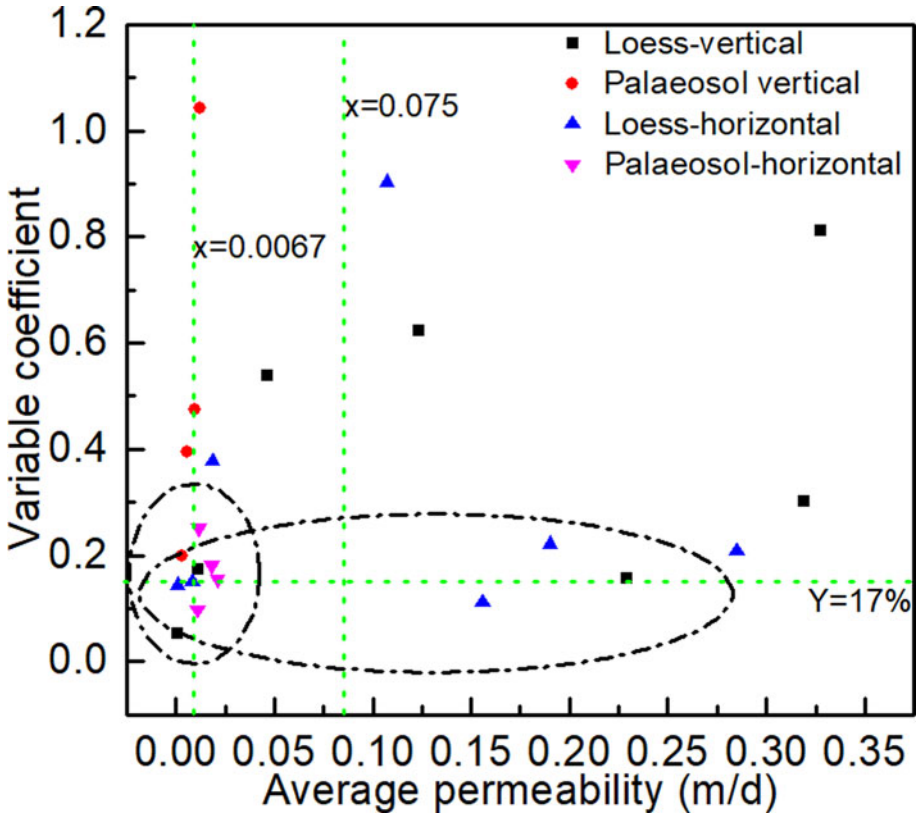

Figure 7 Permeability coefficient variability analysis.

4. Discussion

4.1. Differences in permeability between the loess and palaeosol

From the results of the indoor penetration test, the relationship between the permeability of L_5 and S_5 and the hydraulic gradient showed contrasting characteristics as stratum depth changed. These characteristics can be divided by different strata. As the hydraulic gradient increased, the permeability either: (1) tended to decrease and become stable; (2) decreased until it reached a stable value, then tended to increase; (3) tended to increase in a stable manner; or (4) had no obvious relationship or showed inconsistent characteristics in the horizontal and vertical permeability.

Condition 1 appeared in the upper part of L_5 (L_{5-1}, L_{5-2}, L_{5-3}, L_{5-6}) and in the lower part of S_5 (S_{5-3}, S_{5-4}) (Fig. 10a). This result can be explained by the fact that as the hydraulic gradient increased, fine grains that had been homogeneously distributed in the sample migrated in the direction of seepage, which, in turn, made the void ratio of the sample increasingly heterogeneous. According to the average permeability of the vertical heterogeneous interface flow, the permeability for the whole sample was determined by the single-layer minimum permeability plane. Thus, during this permeability test, the permeability gradually decreased as the hydraulic gradient increased within a certain range. Further, the upper part of L_5 and the lower part of S_5 were at the end of the glacial period or at the outset of the interglacial period and were, therefore, subject to local deposition and climate, particularly at the initial point during which the East Asian summer monsoon (EASM) surged (Zeede *et al*. 2017). During this period, the desert in the Loess Plateau retreated to the NW and the dust grain size became smaller. In this case, fine grains were gradually deposited in the upper part of L_5 and the lower part of S_5 (Guo *et al*. 2000; Dalai *et al*. 2002; Zhao *et al*. 2012a). Moreover, the direction of seepage was the same as that of deposition. Thus, during this permeability

Table 1 Permeability coefficients of L_5–S_5 in a Loess section of the XSD.

	A ($m\,d^{-1}$)		B ($m\,d^{-1}$)		C ($m\,d^{-1}$)	
Column	Vertical	Horizontal	Vertical	Horizontal	Vertical	Horizontal
L5-1	0.16969662	0.22273853	0.16561294	0.15631083	0.06141440	0.03042157
L5-2	0.03025413	0.03934244	0.02959773	0.06073634	0.01034758	0.02550326
L5-3	0.01574171	0.00375543	0.01240127	0.00846135	0.00957238	0.00859036
L5-4	0.33342418	0.30987805	0.27649222	0.17823651	0.42561719	0.20324441
L5-5	0.23937217	0.27315022	0.17056405	0.24277045	0.52261591	0.33886053
L5-6	0.33322873	0.19145477	0.23413010	–	0.21960184	–
L5-7	0.00105100	0.00135000	–	–	–	–
S5-1	0.00443385	0.01171810	–	–	–	–
S5-2	0.00378341	0.01171810	–	–	–	–
S5-3	0.00599180	0.00911594	0.00666068	0.01332843	0.00429842	0.00960025
S5-4	0.01533863	0.01205309	0.01207407	0.01162890	0.00654390	0.01069725

https://doi.org/10.1017/S1755691020000110 Published online by Cambridge University Press

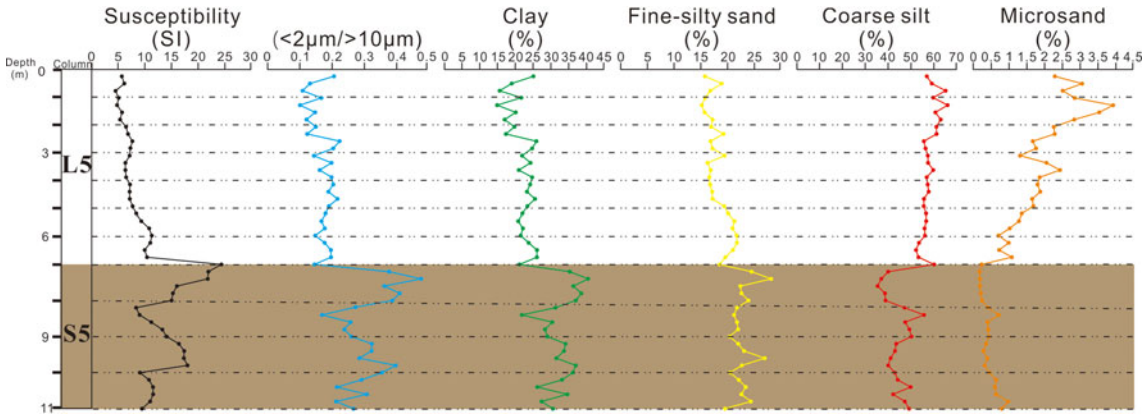

Figure 8 Susceptibility and grain-size curve from L_5–S_5 of a loess section of the XSD.

test and under a higher hydraulic gradient, the permeability in the upper part of L_5 and in the lower part of S_5 gradually became stable.

Condition 2 appeared in L_{5-4}. When the hydraulic gradient was $I \leq 4$, L_{5-4} showed characteristics consistent with Condition 1. However, the permeability tended to increase as the hydraulic gradient increased. Magnetic susceptibility and grain-size analysis indicated that this layer was deposited under a dry-cold climate and was located near the centre of the entire L_5 layer (Reyaz *et al*. 2015). This finding implied that L_{5-4} was nearly surrounded by the East Asian winter monsoon (EAWM) effect during the sedimentary period. Consequently, the weathering and pedogenesis was too weak to form a macroporous support structure. When sample images were compared before and after permeation, along with the subsequent activity of insects in the soil layer, some soluble substances were filled in. Therefore, when the hydraulic gradient was higher ($I > 4$), the fill substances were flushed off, and permeability increased with the hydraulic gradient (Fig. 10b).

Condition 3 appeared in L_{5-5}, with variability similar to that observed in Condition 2 under a higher hydraulic gradient. The table clearly shows that the initial permeability in L_{5-5} was very close to that in L_{5-4} when it was stabilising, and L_{5-5} was deposited before L_{5-4}. Judging from the magnetic susceptibility data, during the transition period from L_{5-5} to L_{5-4}, the intensity of the EAWM gradually weakened, thus reducing the content of large grains that controlled the pore size. Therefore, under the same hydraulic gradient, L_{5-5} stabilised before L_{5-4}, and L_{5-5} may be treated as a special condition of L_{5-4} in which it is under a larger hydraulic gradient. Soil formation involves weathering of the parent material and transformations and translocations of what is within the material, which results in changes of particle size. While the intensity of the winter monsoon has an impact on soil formation, it is not the only factor.

Condition 4 appeared in the lower part of L_5 and in the upper part of S_5. In terms of the position of deposition, these sampling points were in the transition zone from the palaeosol to the loess and had similar sedimentary characteristics. The intensity of the EASM gradually weakened, whereas that of the EAWM began to strengthen (Wang 2005; Zhang *et al*. 2013). As suggested in Figure 7, the intensity of the EASM not only weakened but also tended to fluctuate, which resulted in a heterogeneous material structure in the depositary layer. Further, the soil leaching effect caused a sharp contrast in permeability between the bottom and lower part of L_5 and the sedimentary layer above it.

The permeation process in the samples was not solely influenced by the climate (Jiang *et al*. 2016; Yang *et al*. 2017). According to the analysis of variability, the stable permeability of S_5 was not only poorer, it was also relatively stable as the hydraulic gradient increased, especially in the vertical direction. However, L_5 showed the opposite characteristics, with the condition appearing at the bottom of L_5, in which the permeability was unstable as the hydraulic gradient changed. To further examine the causes of these differences, samples were obtained from the permeameter after the completion of the permeability test (Fig. 10c), and visible wormholes and fissures had appeared after the completion of the permeability test on L_5. This finding indicated that the biological effects of the soil are also an important factor influencing its permeability. Given that biological effects are not cyclical like the Quaternary climate, the relationship between

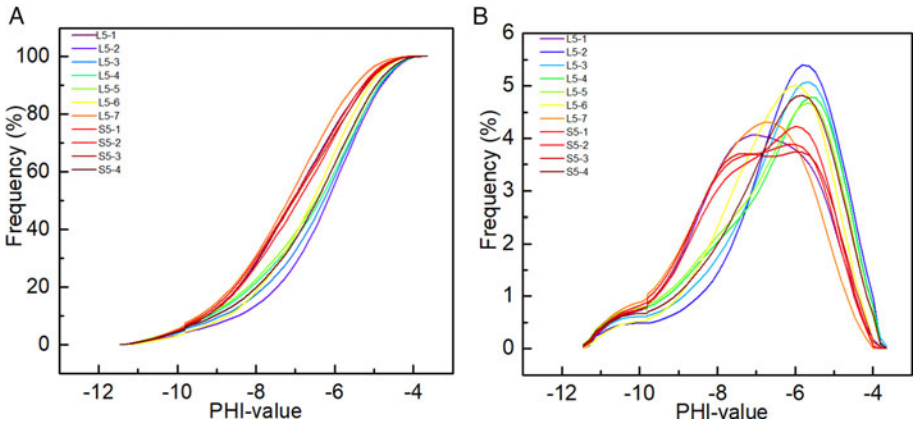

Figure 9 Grain-size distribution and cumulative grain-size distribution curves for L_5 and S_5 of a loess section of the XSD. (A) Probability cumulative grain-size distribution curves and (B) probability grain-size distribution curves.

https://doi.org/10.1017/S1755691020000110 Published online by Cambridge University Press

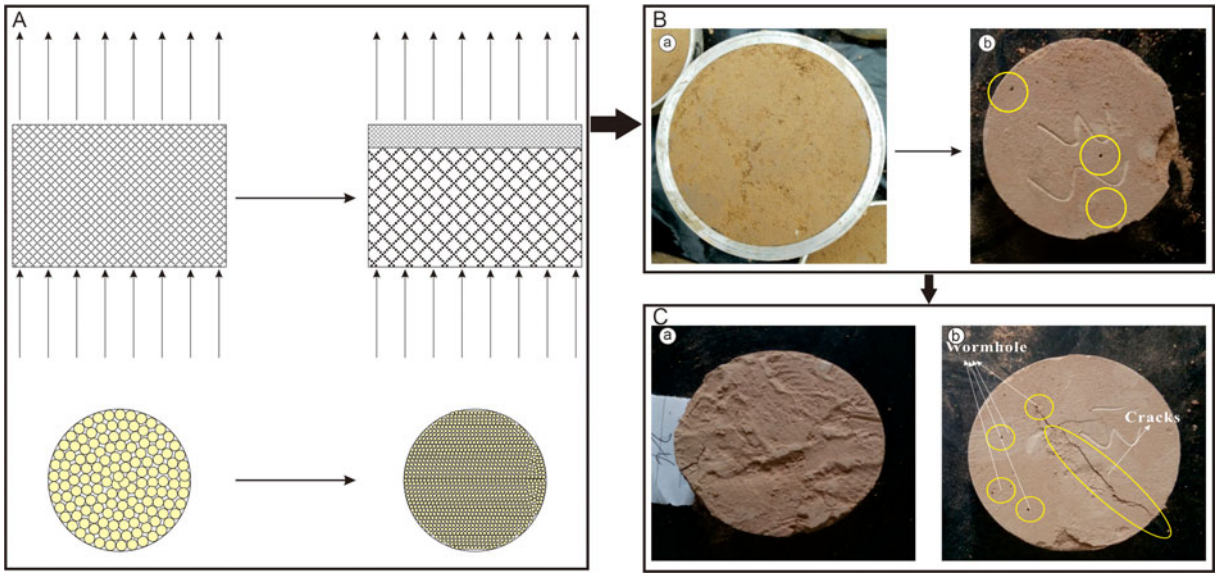

Figure 10 (A) Simulation diagrams of the loess samples during the long-term penetration test; (B) comparison of samples (a) before and (b) after infiltration; (C) comparison of (a) palaeosol and (b) loess.

the palaeosol and the loess in terms of permeability and hydraulic gradient becomes increasingly unstable.

In summary, the permeability of the fifth loess–palaeosol sequence was correlated to the climate. Climatic changes were accompanied with different materials, structures, and grain-size compositions, which, in turn, caused contrasting permeability characteristics under different hydraulic gradients. In addition, there was an uncertain biological effect from the soil immediately followed by unstable permeability, which changed with the hydraulic gradient during the permeation process. In this sense, the permeability differences in the loess–palaeosol sequence can be used as a reference index for changes in the climate and the biological environment.

4.2. Influence of material structure characteristics of the stratum on permeability

Previous studies on loess–palaeosol sequences have suggested that the grain-size composition can be used as an alternative index for indicating changes in climate and the intensity of weathering and pedogenesis (Guo *et al.* 2000; Singh *et al.* 2008; Liu *et al.* 2015). As described earlier, finer-grain components migrated along the direction of seepage during the permeation process, which resulted in changes in the coefficient of permeation. In addition, the grain-size composition also had a great influence on the stability of the permeability of the loess–palaeosol sequence.

As shown in Table 1 and Figure 9, during the evolution process from L_5 to S_5, the ratio of grains that were smaller than 2 μm and greater than 10 μm were regarded as the result of index analysis, which tended to increase. The content of clay and fine-silty sand gradually decreased, as did the stable permeability in each layer of the study profile. This observation can be attributed to the fact that as fine-grain content increases, it often results in smaller pore sizes in the sedimentary layer, lower porosity, higher dry density (Fig. 4), and weaker connectivity of pores, which, in turn, cause the stable permeability to decrease. Compared to S_5, there were coarser grains in L_5, ensuring that L_5 had higher porosity, larger pore size, and better connectivity between effective pores, which, in turn, caused the stable permeability to increase.

Similarly, given that the moisture in the loess–palaeosol sequence mainly existed in the form of film water, the content of clay and fine-silty sand was higher in S_5 (Fig. 4) and the stratum had a stronger absorption (Xu & Zhao 2002; Fu *et al.* 2018; Chen *et al.* 2020a, b), which reduced the stable permeability during the permeation process. Compared to S_5, the content of clay and fine-silty sand in L_5 was lower, but the content of coarse silt and microsand was higher, the soil absorption was weaker, and the moisture content was lower, which, in turn, caused the stable permeability to be greater than that of S_5.

This analysis showed that the grain-size composition of the soil largely determines the physical and hydraulic properties of the loess–palaeosol sequence, which, in turn, influences permeability.

4.3. Differences in aquifers of the loess–palaeosol sequence as a result of climate change

According to field observations, almost no $CaCO_3$ nodules were found in L_5 and the magnetic susceptibility curve was relatively flat, which indicated that L_5 was deposited under a climate with less precipitation and pedogenesis. In S_5, there were more $CaCO_3$ nodules and the magnetic susceptibility curve often formed prominent peaks, indicating that S_5 was deposited under a climate with abundant precipitation and a stronger leaching effect (Wang 2005; Zhao *et al.* 2017).

Chemical weathering is often done via water; thus, it is almost impossible to observe under a dry environment (Zhao *et al.* 2012b). Therefore, S_5 deposited during the humid-warm interglacial period showed a stronger leaching effect, contained more enriched ferromagnetic minerals, and had a higher magnetic susceptibility (Huang *et al.* 2009). However, the weathering effect in the loess was weaker under the dry-cold climate, causing lower magnetic susceptibility (Zhao *et al.* 2015). According to the comparison between the porosity curve and the magnetic susceptibility curve, L_5 had a lower magnetic susceptibility value and a higher porosity, whereas S_5 had a higher magnetic susceptibility value and a lower porosity. Differences in porosity between L_5 and S_5 may have been primarily caused by the dominant climate at the time of deposition. The surface the difference between these things types of loess, cementing the grains around the pores that were built when windblown dust fell down and fixed them in a very loose structure. In this way, overhead large pores can be easily formed in the loess. After being compressed by the overlying stratum, the palaeosol grains with more clay were filled with clay, leaving some small pores between them (Fang *et al.* 2017).

The pores in loess soil were mainly formed during their formation. The intensity of pedogenesis is directly correlated to the

https://doi.org/10.1017/S1755691020000110 Published online by Cambridge University Press

climate. During the sedimentary period of the loess under a relatively dry-cold climate, the clarification was weaker, and there were no cements between deposited grains, resulting in the development of an aquifer between the grains. During the formation of the palaeosol, the climate was relatively humid-warm, as the EASM in the SE direction was enhanced and the desert in the Loess Plateau retreated to the NW, making the dust grains increasingly fine. The combined effects of high temperature, high precipitation, and fine grains resulted in strengthened clarification in the palaeosol, mutually cemented grains, and reduced porosity, which, in turn, enhanced its water-resistant properties. The experimental results showed that although the porosity of S_5 was lower than that of L_5, it was still high. In this sense, the water-resistant properties of the palaeosol were only relative to that of loess, and may still become permeable under certain conditions.

In summary, the differences in aquifer properties between the loess–palaeosol sequence result from the cyclic impacts between EASM and EAWM.

5. Conclusions

(1) In the loess–palaeosol sequence of the XSD profile, as the hydraulic gradient increased, different experimental points showed inconsistent characteristics due to environmental differences during the deposition period. However, the strata, subject to similar monsoon effects, shared certain similarities.

(2) Subject to the dominant effect of the alternating cycles of the EASM and EAWM, the differences in grain-size composition between the loess–palaeosol sequence under the sedimentary environment was the primary cause for the different values of stable permeability in different stratum. Moreover, the stable permeability of the loess, which is mainly composed of coarse grains, was significantly higher than that of the palaeosol, which is mainly composed of fine grains.

(3) The aquifer in the loess was more deposited than that in the palaeosol as it is closely associated with the alternating cycles of dry-cold and humid-warm climates during the Quaternary period. The loess formed during the dry-cold glacial period showed a weak soling effect. The deposited grains, which were relatively coarse, formed large pores with stronger permeability and larger aquifer, which was conducive to recharge.

6. References

Allen, J. R. M., Brandt, U., Brauer, A., Hubberten, H. W., Huntley, B., Keller, J., Kraml, M., Mackensen, A., Mingram, J., Negendank, J. F. W., Nowaczyk, N. R., Oberhänsli, H., Watts, W. A., Wulf, S. & Zolitschka, B. 1999. Rapid environmental changes in Southern Europe during the last glacial period. *Nature* **400**, 740–43.

An, Z., Wu, G., Li, J., Sun, Y., Lu, Y., Zhou, W., Cai, Y., Duan, A., Li, L., Mao, J., Cheng, H., Shi, Z., Tan, L., Yan, H., Ao, H., Chang, H. & Feng, J. 2015. Global monsoon dynamics and climate change. *Annual Review of Earth and Planetary Sciences* **43**, 29–77.

Balsam, W., Ji, J. & Chen, J. 2004. Climatic interpretation of the Luochuan and Lingtai loess sections, China, based on changing iron oxide mineralogy and magnetic susceptibility. *Earth and Planetary Science Letters* **223**, 335–48.

Chen, J., Wu, H. & Qian, H. 2016. Groundwater nitrate contamination and associated health risk for the rural communities in an agricultural area of Ningxia, northwest China. *Exposure and Health Volume* **8**, 349–59.

Chen, J., Qian, H. & Wu, H. 2017. Nitrogen contamination in groundwater in an agricultural region along the New Silk Road, northwest China: distribution and factors controlling its fate. *Environmental Science and Pollution Research* **24**, 13154–67.

Chen, J. & Qian, H. 2017. Characterizing replenishment water, lake water and groundwater interactions by numerical modeling in arid region a case study of Shahu Lake. *Hydrological Sciences Journal* **62**, 104–13.

Chen, Y., Li, X., Han, Z. & Yang, S. 2008. Chemical weathering intensity and element migration features of the Xiashu loess profile in Zhenjiang, Jiangsu Province. *Journal of Geosciences* **18**, 341–52.

Chen, Y., Huo, W. X., Qian, H. & Li, B. C. 2020a. Research on Holocene loess erosion associated to climate evolution in China. *Polish Journal of Environmental Studies* **1**, 409–17.

Chen, Y., Qian, H., Hou, K., Zhang, Q. Y. & Zhang, Y. T. 2020b. Vertical distribution characteristics of soil moisture with different strata in deep profile in Guanzhong Basin, China. *Environmental Earth Sciences* **79**, 103.

Dalai, T. K., Krishnaswami, S. & Sarin, M. M. 2002. Major ion chemistry in the headwaters of the Yamuna river system: chemical weathering, its temperature dependence and CO_2 consumption in the Himalaya. *Geochimica et Cosmochimica Acta* **66**, 3397–416.

Fang, Q., Hong, H., Zhao, L., Furnes, H., Lu, H., Han, W., Liu, Y., Jia, Z., Wang, C., Yin, K. & Algeo, T. J. 2017. Tectonic uplift-influenced monsoonal changes promoted hominin occupation of the Luonan Basin: insights from a loess-paleosol sequence, eastern Qinling Mountains, central China. *Quaternary Science Reviews* **169**, 312–29.

Fu, C. F., Bian, Z. H., Xi, J. J. & Zhao, J. B. 2018. Spatial distribution characteristics of soil moisture in different types of sand dune in the Mu Us Sandy Land, adjacent to north of Chinese Loess Plateau. *Environmental Earth Sciences* **77**, 151.1–151.12.

Gorbarenko, S. A., Goldberg, E. L. V., Kashgarian, M., Velivetskaya, T. Y. A., Zakharkov, S. P., Pechnikov, V. S., Bosin, A. A. E., Psheneva, O. Y. E. & Ivanova, E. D. 2007. Millenniumm scale environment changes of the Okhotsk Sea during last 80 kyr and their phase relationship with global climate changes. *Journal of Oceanography* **63**, 609–23.

Guo, Z., Biscaye, P., Wei, L., Chen, X., Peng, S. & Liu, T. 2000. Summer monsoon variations over the last 1.2 Ma from the weathering of loess-soil sequences in China. *Geophysical Research Letters* **27**, 1751–54.

Huang, C. C., Pang, J., Su, H., Li, S. & Ge, B. 2009. Holocene environmental change inferred from the loess-palaeosol sequences adjacent to the floodplain of the Yellow River, China. *Quaternary Science Reviews* **28**, 2633–46.

Huang, T., Pang, Z. & Edmunds, W. M. 2013. Soil profile evolution following land-use change: implications for groundwater quantity and quality. *Hydrological Processes* **27**, 1238–52.

Jiang, H., Guo, G., Cai, X., Thompson, J. A., Xu, H. & Zhong, N. 2016. Geochemical evidence of windblown origin of the Late Cenozoic lacustrine sediments in Beijing and implications for weathering and climate change. *Palaeogeography, Palaeoclimatology, Palaeoecology* **446**, 32–43.

Kukla, G., Heller, F., Liu, X. M., Xu, T. C., Liu, T. S. & An, Z. S. 1998. Pleistocene climates in China dated by magnetic susceptibility. *Geology* **16**, 811–14.

Kukla, G. & An, Z. S. 1989. Loess stratigraphy in central China. *Palaeogeography, Palaeoclimatology, Palaeoecology* **72**, 203–25.

Li, P. Y., Qian, H., Wu, J. H., Zhang, Y. Q. & Zhang, H. B. 2013a. Major ion chemistry of shallow groundwater in the Dongsheng Coalfield, Ordos Basin, China. *Mine Water and the Environment* **32**, 195–206.

Li, P. Y., Wu, J. H. & Qian, H. 2013b. Assessment of groundwater quality for irrigation purposes and identification of hydrogeochemical evolution mechanisms in Pengyang County, China. *Environmental Earth Sciences* **69**, 2211–25.

Liu, Q. S., Jin, C. S., Hu, P. X., Jiang, Z. X., Ge, K. P. & Andrew, P. R. 2015. Magneto stratigraphy of Chinese loess-paleosol sequences. *Earth-Science Reviews* **150**, 139–67.

Liu, T. S. & Ding, Z. L. 1998. Chinese Loess and the paleomonsoon. *Annual Review of Earth and Planetary Sciences* **26**, 111–45.

Liu, X. 2015. The response of infiltration depth, evaporation, and soil water replenishment to rainfall in mobile dunes in the Horqin Sandy Land, Northern China. *Environmental Earth Sciences* **73**, 8699–708.

Lu, L. Q., Fang, X. M., Lu, H. Y., Han, Y. X., Yang, S. L., Li, J. J. & An, Z. S. 2004. Millennial-scale climate change since the last glaciation recorded by grain sizes of loess deposits on the northeastern Tibetan Plateau. *Chinese Science Bulletin* **49**, 1157–64.

Pan, Y. X., Wang, X. P., Zhang, Y. F. & Rui, H. 2015. Spatio-temporal variability of root zone soil moisture in artificially revegetated and natural ecosystems at an arid desert area, NW China. *Ecological Engineering* **79**, 100–12.

Peng, S. Z., Hao, Q. Z., Frank, O. & Guo, Z. T. 2014. Release of iron from chlorite weathering and links to magnetic enhancement in Chinese loess deposits. *Catena* **117**, 43–49.

Qian, H. & Li, P. Y. 2011. Hydrochemical characteristics of groundwater in Yinchuan plain and their control factors. *Asian Journal of Chemistry* **23**, 2927–38.

Rao, Z., Chen, F., Cheng, H., Liu, W., Wang, G. A., Lai, Z. & Bloemendal, J. 2013. High- resolution summer precipitation variations in the western Chinese Loess Plateau during the last glacial. *Scientific Reports* **3**, e2785.

Reyaz, A. D., Rakesh, C., Shakil, A. R. & Nazia, K. 2015. Micromorphological investigations of the Late Quaternary loess-paleosol sequences of the Kashmir Valley, India. *Journal of Asian Earth Sciences* **111**, 328–38.

Ruddiman, W. F., Raymo, M. F., Martinson, D. G., Clement, B. M. & Backman, J. 1989. Pleistocene evolution: northern hemisphere ice sheet and Northern Atlantic Ocean. *Paleoceanography* **4**, 353–412.

Singh, A. K., Mondal, G. C., Kumar, S., Singh, T. B., Tewary, B. K. & Amalendu, S. 2008. Major ion chemistry, weathering processes and water quality assessment in upper catchment of Damodar River basin, India. *Environmental Geography* **54**, 745–58.

Song, Y. G., Chen, X. L., Qian, L. B., Li, C. X., Li, Y., Li, X. X., Chang, H. & An, Z. S. 2014. Distribution and composition of loess sediments in the Ili Basin, Central Asia. *Quaternary International* **334**, 61–73.

Stevens, T., Thomas, D. S. G., Armitage, S. J., Lunn, H. R. & Lu, H. 2007. Reinterpreting climate proxy records from late Quaternary Chinese Loess Plateau. *Qualitative Research* **64**, 234–41.

Torrent, J., Liu, Q., Bloemendal, J. & Barron, V. 2007. Magnetic enhancement and iron oxides in the upper Luochuan loess-paleosol sequence, Chinese Loess Plateau. *Soil Science Society of America Journal* **71**, 1570–78.

Wang, L. P., Huang, T. T., Yang, G. P., Lu, C.Y., Dong, F.L., Li, Y.L., & Guan, W. S. 2019a. The precursor-guided hydrothermal synthesis of $CuBi_2O_4/WO_3$ heterostructure with enhanced photoactivity under simulated solar light irradiation and mechanism insight. *Journal of Hazardous Materials* **381**, 120956.

Wang, L. P., Yang, G. P., Wang, D., Lu, C.Y., Guan, W.S., Li, Y.L., Deng, J. & John, C. 2019b. Fabrication of the flower-flake-like $CuBi_2O_4/Bi_2WO_6$ heterostructure as efficient visible-light driven photocatalysts: performance, kinetics and mechanism insight. *Applied Surface Science* **495**, 143521.

Wang, S. J. 2005. Perspectives on hominid behaviour and settlement patterns: a study of the lower Paleolithic sites in the Luonan Basin, China. BAR International Series, 1406. Archaeopress, Oxford, 248 pp.

Wang, W. W., Sun Q, Y., Zhang, M., Qiang, Y. & Liu, M. 2018. Spatial variation of saturated hydraulic conductivity of a loess slope in the South Jingyang Plateau, China. *Engineering Geology* **236**, 70–78.

Wang, Z., Wang, L., Liu, L. & Zheng, Q. 2007. Preliminary study on the spatiotemporal distribution of moisture content in sand dunes in the southern marginal zone of the Mu Us Desert. *Arid Zone Research* **24**, 61–65. [In Chinese.]

Wu, H., Li, X. & Qian, H. 2018. Detection of anomalies and changes of rainfall in the Yellow River Basin, China, through two graphical methods. *Water* **10**, 15.

Wu, H., Li, X., Qian, H. & Chen, J. 2019. Improved partial trend method to detect rainfall trends in Hainan Island. *Theoretical and Applied Climatology* **137**, 2539–47.

Wu, H. & Qian, H. 2016. Innovative trend analysis of annual and seasonal rainfall and extreme values in Shaanxi, China, since the 1950s. *International Journal of Climatology* **37**, 2582–92.

Xu, Q. X. & Zhao, J. B. 2002. The change characteristic of moisture content of loess stratum in the Xi'an area. *Geoscience* **4**, 435–38. [In Chinese.]

Yang, Z., Qiao, J., Uchimura, T., Wang, L., Lei, X. & Huang, D. 2017. Unsaturated hydro- mechanical behaviour of rainfall-induced mass remobilization in post- earthquake landslides. *Engineering Geology* **222**, 102–10.

Zeede, C., Hambach, U., Veres, D., Fitzsimmons, K., Obreht, I., Bösken, J. & Lehmkuhl, F. 2017. Millennial scale climate oscillations recorded in the Lower Danube loess over the last glacial period. *Palaeogeography, Palaeoclimatology, Palaeoecology* **2016**, S0031018216309051.

Zhang, F., Jin, Z. & Li, F. 2013. The dominance of loess weathering on water and sediment chemistry within the Daihai Lake catchment, northeastern Chinese Loess Plateau. *Applied Geochemistry* **35**, 51–63.

Zhao, J. B., Cao, J. J., Shao, T. J., Liu, R., Yue, Y. L. & Du, J. 2012a. The discovery and study of silver sulfate mineral in S5 from the eastern suburb of Xi'an. *Science China Earth Sciences* **55**, 456–63.

Zhao, J. B., Long, T. W., Wang, C. Y. & Zhang, Y. 2012b. How the Quaternary climatic change affects present hydrogeological system on the Chinese Loess Plateau: a case study into vertical variation of permeability of the loess-palaeosol sequence. *Catena* **92**, 179–85.

Zhao, J. B., Ma, Y. D., Cao, J. J., Wei, J. P. & Shao, T. J. 2015. Effect of Quaternary climatic change on modern hydrological systems in the southern Chinese Loess Plateau. *Catena* **73**, 1161–67.

Zhao, J. B., Ma, Y. D., Luo, X. Q., Yue, D. P., Shao, T. J. & Dong, Z. B. 2017. The discovery of surface runoff in the megadunes of Badain Jaran Desert, China, and its significance. *Science China Earth Sciences* **60**, 707–19.

MS received 12 July 2019. Accepted for publication 26 August 2020. First published online 10 November 2020